6-23-2020

Investigation of deformation induced micro to macro scale surface roughness

Ayotunde Olayinka
University of Louisiana

William J. Emblom
University of Louisiana

Scott W. Wagner
Michigan Technological University, swwagner@mtu.edu

Michael Khonsari
Louisiana State University

Ali Haghshenas
Louisiana State University

Recommended Citation

Olayinka, A., Emblom, W. J., Wagner, S. W., Khonsari, M., & Haghshenas, A. (2020). Investigation of deformation induced micro to macro scale surface roughness. *Procedia Manufacturing, 48*, 237-243. http://doi.org/10.1016/j.promfg.2020.05.043
Retrieved from: https://digitalcommons.mtu.edu/michigantech-p/2818

Follow this and additional works at: https://digitalcommons.mtu.edu/michigantech-p

 Part of the Mechanical Engineering Commons

Available online at www.sciencedirect.com

ScienceDirect

Procedia Manufacturing 48 (2020) 237–243

Procedia MANUFACTURING

www.elsevier.com/locate/procedia

48th SME North American Manufacturing Research Conference, NAMRC 48 (Cancelled due to COVID-19)

Investigation of Deformation Induced Micro to Macro scale Surface Roughness

Ayotunde Olayinka[a,*], William J. Emblom[a], Scott W. Wagner[b], Michael Khonsari[c], Ali Haghshenas [c]

[a]*Mechanical Engineering University of Louisiana at Lafayette, 241 E. Lewis St., Lafayette, LA 70503*
[b]*Mechanical Engineering, Michigan Tech, 1400 Townsend Drive, Houghton, MI 49931*
[c]*MechanicalEngineering, 3261 Patrick F. Taylor Hall, Louisiana State University, Baton Rouge, LA 70803*

* Corresponding author. Tel.: +1-337-255-3205; *E-mail address:* ayotunde.olayinka1@louisiana.edu

Abstract

In the present work the relationship between deformation and deformation induced surface roughness of 100 micron thick annealed AISI 304 stainless steel was investigated at the meso scale. This work is a continuation of the previous work by the authors where roughness values were determined at the apex of the bulge test samples at micro scale. The apex is believed to be the region of highest stress and strain in a typical bulge process in a circular die. The material was deformed using a biaxial bulge test through hydraulic fluid pressure. The strains on the workpieces were measured with respect to the forming pressure. The surface roughness was measured by scanning the interior (concave) area of bulge with Bruker GTK-17 optical profilometer over an area of 1.3mm x 1mm. The results show linear relationship between roughness and deformation strain, and it establish a similar trend with roughness measured at micro scale.

Keywords: Hydroforming; surface roughness; sheet metal forming; optical profilometry

1. Introduction

Hydroforming is a cost-effective metal forming operation that uses a pressurized fluid to hydrostatically deform materials into desired a shape or form. Generally, micro scale forming encompasses production processes where at least two of the dimensions are in the submillimeter range [1-3], and micro hydroforming is one technique that has gained traction in the manufacturing of micro scale devices in recent years [4-7]. In the present work, the relationship between the deformation strain and deformation induced surface roughness was investigated at a meso scale level. For small scale applications, surface roughness becomes very important in situations where contacting parts are involved it affects surface characteristics such as wear resistance and resistivity of materials. Grain size, anisotropy, initial roughness, state of stress, inclusions, crystal structures, and effective deformation are some of the factors that are known to determine surface roughness of metallic parts [8]. Microscale roughness in micro-scale hydroforming was investigated by Olayinka et al. [9]. They scanned the apex of the bulge of hydroformed 200 micro thick stainless steel using atomic force microscope at microscale. They observed that a linear relationship can be established between the strain and the surface roughness. Timoshevscii et al. [10] investigated the effect of atomic scale surface roughness on conductivity of very thin copper foil. They found that small roughness of only few atoms resulted in about 30-40% reduction of the electrical conductivity. They attributed this reduction to intersheet electron scattering at the Fermi surface, which is the result of roughness. The effect of size effect phenomenon on the surface roughness has been studied by Meng et al. [11,12] who concluded that the ratio of free surface roughening increases as the thickness decreases. In their study, Raabe et al.[13, 14] attributed the cause of roughness to grain boundary

10.1016/j.promfg.2020.05.043

disorientation or mismatched hardness of neighboring grains. LSDYNA incorporated with a rate dependent crystal plasticity model was used by Rossiter et al. [15] to analyze some selected FCC metals. They found that the surface roughness shows a direct relationship to the difference in strain accommodating capabilities in different orientations within a polycrystal aggregate. The roles of Taylor's factor, grain boundary misorientation, large Schmidt factors, grain sizes, coincidental lattice orientation, and local grain break ups in the deformation induced surface roughness of polycrystalline aluminium AA6602 were studied by Stoudt et al. [16]. They found that the concentration of the largest surface displacement was observed in regions where there are large differences between the Taylor's factors and individual grains.

Forming sheet metals into different desired shapes through various forming methods is through plastic deformation. When plastic deformation occurs, changes do not just occur in the macroscale shape or sizes but there are also changes in the microscale and the atomic level of the metal [17]. The microscopic constituents of such metals could be in the form of defects such as imperfection, inclusions, and voids. Plastic deformation occurs through slipping of atoms along an identified crystal planes in a specified crystal structure. This slipping occurs through the linear movement of the lattice defects referred to as dislocations. Grain boundaries, internal defects and surface irregularities serve as formation sites for dislocations during deformation. Grain boundaries separate crystals from each other, they are produced during solidification of metals, and their orientation is chaotic, this allows them to impede the movement of dislocations [18,19]. These slips are determined by the crystal structures. The motion of the dislocation transports atoms from one equilibrium position to another. The microstructure of metal is known to evolve with increasing strain and is believed to result in changes in micro surface roughness of the metallic material [16, 20]. The understanding of these behaviors of metals are very important in the study of plastic deformation induced roughness in metallic materials. It will also play a very important role during fabrication of metallic parts especially in the microscale and mesoscale.

The primary goal of this research is to investigate formability of annealed AISI 304 for application in bipolar plates for proton exchange membrane fuel cells (PEMFC). One of the major challenges encountered in the development of metallic bipolar plates for PEMFC has been to determine how to improve the quality and durability while reducing the cost of manufacturing. It has been reported that fabrication technique considerably impacts on the cost of bipolar plates manufacturing [21]. In their previous work [9] the authors established relationship between formability and surface roughness at microscale level. The present work studies the effects of the hydroforming manufacturing technique on the relationship between plastic deformation and macroscale surface roughness in a 0.1mmthick annealed AISI 304 stainless steel using bulge testing method. Surface roughness is a very important factor for the functionality of metallic bipolar plates as it affects conductivity (electrical and thermal), water management, and corrosion characteristics of a bipolar plate. This work will provide insight into applications that involve micro to macro scale contact such as the interaction between bipolar plates and gas diffusion layers in a typical proton exchange membrane fuel cell (PEMFC) because the actual microscopic contacts are made between asperities of the contacting surfaces. Likewise, this current project is also valid for other micro flow channeling applications such as medical devices and micro heat exchangers.

2. 1 Materials

The material chosen for this study is 100 μm thick annealed AISI 304 stainless steel (Brown Metals Company, USA). AISI 304 stainless steel is an austenitic stainless steel with FCC crystal structure. Stainless steel is used in various applications ranging from cooking ware to machinery and automobile parts. They have very impressive corrosion resistance in chloride and sulphate, and other oxidizing environments. The AISI 304 stainless steel is annealed in order to enhance its formability. Flat 38 mm by 38 mm square specimens were cut from the blank stock. The percent compositions of the stainless-steel material include 0.015 C, 1.57 Mn, 0.031 P, 0.001 S, 0.41 Si, 18.18 Cr, 9.06 Ni, 0.35 Mo, 0.56 Cu, 0.04 N, 0.18 Co, with the balance being Fe. The mechanical properties provided by the manufacturer are shown in Table 1.

Table 1. Mechanical Properties.

Material Properties	Value	Unit
Yield Strength	274	MPa
Tensile Strength	635	MPa
Elongation	88	Percent
Hardness	149	HV
Strain Exponent	0.4	
Poisson Ratio	0.33	

2.2. Meso/micro scale hydraulic bulge test set-up and procedure.

The formability of materials is often studied by investigating the material behavior under biaxial stress conditions resulting from hydraulic bulge processes. The hydraulic bulge test set-up consists of a calibrated pump system from which pressure was exerted and measured using a pressure gauge attached to the pressure intensifier. A 60-ton Baldwin press was used to apply the clamping force through the upper tooling in order to hold the work pieces in place against 5 mm diameter hole in the lower tooling. The illustration of the die system is as shown in Figure 1. The 5-mm circular die used in this study was fabricated from D2 tool steel that had been hardened (58 RC). The holes were cut by wire EDM at the center of the die. The hydraulic bulge test can attain higher plastic strains before instability sets in compared to other conventional material testing technique such tension test. In addition, the hydraulic bulge test also has the advantage in that the strain at the pole of the bulge can be determined analytically by accurate measurement of the height of the dome and the diameter of the die. Previous studies have shown that effective stress can be determined using the bulge or dome height during hydraulic bulge test [7, 22]. Three samples each were made for each

hydraulic forming pressure used for this study. The test pressures considered in Psi are 1500, 3000, 4500, 6000 and 6900 (this is the pressure in the vicinity of burst)

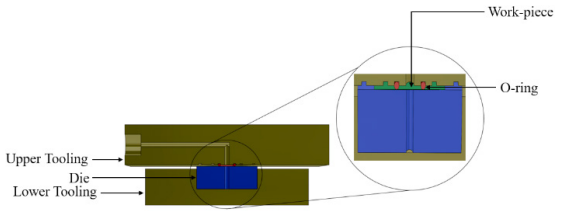

Fig. 1. Schematic of the hydroforming tooling system

A stepwise technique with respect to pressure was used to determine the dome height of the bulge. The workpieces were centred on the die and a 20-mm Viton O-ring was positioned in the groove within the upper tooling was used to create sealing between the upper tooling and the blank. A blank holding force was exerted by the press. The pressurized hydraulic fluid flows through the upper tooling to the workpieces. The peak pressure was measured and recorded during each test using the pressure gauge installed on the pressure intensifier. Once the desired bulging pressure was attained, the test was stopped, and the specimen was removed. The dome height was measured for each test using a digital micrometer (Mitutoyo, Japan).

2.3. Experimental determination of strain.

The determination of thickness along the dome of the formed samples was done by cutting the sample in the vicinity of the mid plane using a precision machine Isomet 1000 (Buehler, USA). This prevented the deformation of the sectioned face. The sectioned halves were mounted in a clear epoxy resin. The mounted samples were grounded using silicon oxide abrasive paper (Buehler, USA) grid 320 to 4000, samples were subsequently mechanically polished. Axiostech compound microscope (Carl Zeiss, USA) was used to enlarge the image of the sectioned surface to the magnification of 200X as shown in Figure 2. The point of interest for this study in indicated by the red ring in Figure 2. The images were captured with digital camera D7000 (Nikon, Japan) that was attached to the microscope. The digital image captured were analyzed with digital image software ImageJ.

Fig. 2. Cross section of hydroformed specimen

2.4 Microstructural evaluation.

Microscopic imaging using a JSM 6300F field emission scanning electron microscope (JEOL, USA) of a work piece that had undergone burst was done in order to examine the microscopic detail of the fractured surface in order to characterize the nature of deformation. The samples fractured at the dome of the samples as indicated by the red ring in Figure 2

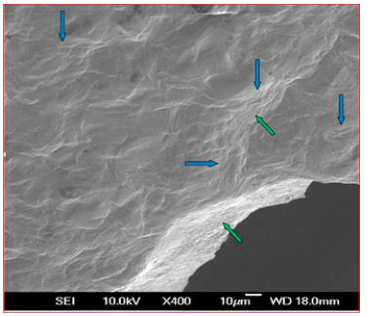

Fig. 3. SEM images of fractured surface showing striation (green) and crystallographic slip planes (blue). (Olayinka et al., 2017)

This is an indication as to the nature of deformation of the subject material. The fractured surface of stainless-steel sample at failure shown in Fig. 3 shows that the sample's mode of failure is ductile failure. This suggests that material during bulge test is under tension through stretching. The blue arrows indicate crystallographic slip planes and it shows the direction of slip. The presence of striation on the fractured surface are indicated by the green arrows.

2.5. Surface roughness.

The samples used for this study are made from annealed AISI 304 stainless steel that have been hydroformed at varying pressures using a 5-mm diameter die. Each of the samples was rinsed with acetone to remove small contaminants that might interfere with the scans. The rinsed and degreased samples were dried in the air and subsequently wiped using denatured spirit. The initial images of the samples were taken at a magnification of 50x using a digital microscope (Cool-Tech, China). The images are shown in Fig. 4.

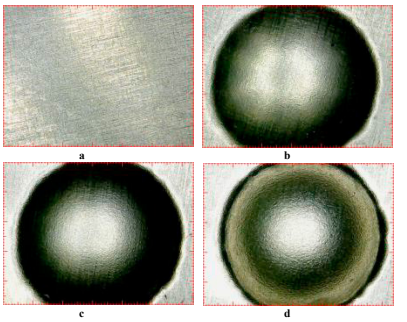

Fig. 4. Digital microscope image (a) plane (b) 10.34 MPa (c) 20.68 MPa (d) 44 MPa (50X)

The 3D optical profilometer GTK-17 (Bruker, USA) was used to determine the roughness parameters of the sample surfaces. The optical profilometer measures 3D surfaces by means of white light interferometry. The parameters of the optical profilometer are shown in Table 2. The samples were positioned carefully on the sample stage of the profilometer in order to ensure the surface is in focus. Fig. 5 shows the results of the roughness mapping for the "as received" sheet and the

hydroformed samples.

Table 2. Contour GT-X profilometer parameters settings

Parameters	Values	Unit
Vertical resolution	<0.1	nm
Lateral resolution	2	µm
Step height accuracy	<0.75	Percent
Measurement type	VXI	
Objective	5x	
Magnification	40	
Measurement area	1	mm

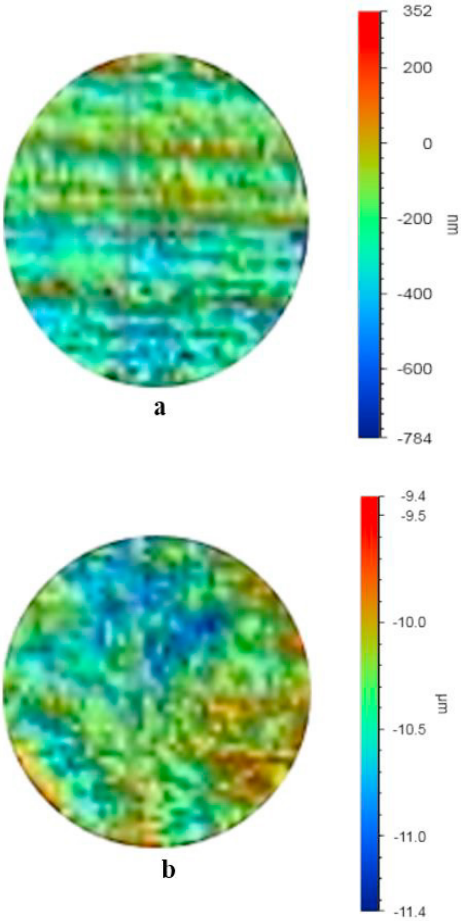

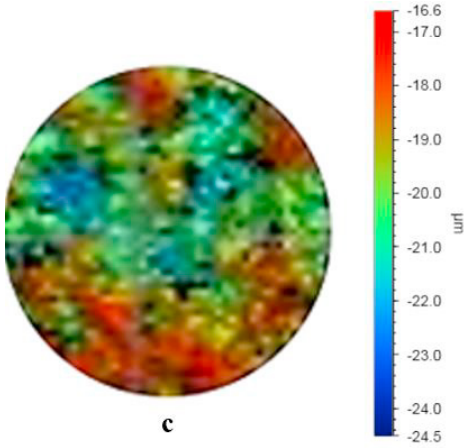

Fig. 5. Roughness map (a) as received surface (b) 10.34 MPa (c) 41.37 MPa

Figure 5 shows progression in roughening of the samples as the applied hydraulic pressure increases from 0 MPa to 41.37mPa

3. Results and Discussion

3.1 Bulging test results.

Fig. 6 shows the power law relationship between the pressure and the dome height for stainless steel samples that deformed plastically inside a 5 mm hole cavity die under hydraulic fluid pressure. The result was obtained by measuring the vertical deflection of the sample piece after the selected stepwise bulge pressure have been attained. The maximum value of pressure attained during the stepwise bulging test was 44.13 MPa, this pressure is in the vicinity of the burst pressure for the bulge test's 5-mm die diameter. The corresponding polar deflection or dome height at this pressure was 1.73 mm.

The maximum stresses and strains were located at the pole of the dome, the localized biaxial stress state at the pole resulted in reduction in metal thickness until failure occurred. However, in some instances such when as insufficient blank holding forces or through instability caused by variations of the cross

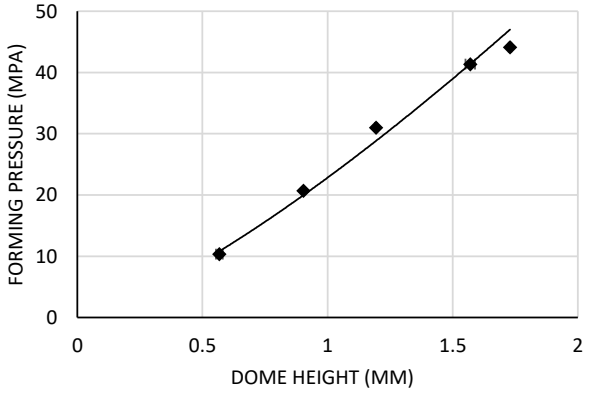

section, failure could be away from the pole.

Fig. 6. Plot of forming pressure for various dome heights

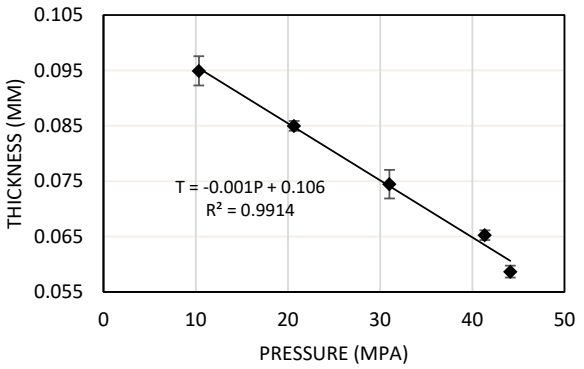

Fig. 7. Plot of pole thickness for various pressures

The result in Fig. 7 indicates that as the hydraulic pressure and the dome height increases the thickness at the pole of the dome decrease. This can be reinforced by sample cross-section shown in Fig. 2.

3.2 Surface roughness

S_a is the extension of R_a the average roughness to a surface, it is used generally to evaluate surface roughness. S_q represents the root mean square value of ordinate values within the definition area. It is equivalent to the standard deviation of heights. S_a and S_q are the Average Roughness and Root Mean Square Roughness are evaluated over the complete 3D surface respectively. S_q is typically used to specify optical surfaces and S_a is used for machined surfaces. Mathematically, S_a and S_q are represented in Equations (1) and (2) respectively:

$$S_a = \iint_a |Z(x,y)|\,dx\,dy \quad (1)$$

$$S_q = \sqrt{\iint_a Z(x,y)^2\,dx\,dy} \quad (2)$$

S_z is defined as the sum of the largest peak height value and the largest pit depth value within the defined area**.** R_a measurements look at the smoothness of a sliding surface and R_z measurements look at the surface height. Because using R_a alone may cause some points, such as single protrusions, to be overlooked it is important that both S_a and S_z be used together. Typical applications for S_z may include sealing surfaces and coating applications, while, S_v may found application when valley depths relating to fluid retention may be of concern such as for lubrication and coating systems.'

The variation of roughness different parameters and effective strain are described in Fig. 8. All the parameters show similar trends to increase in strain. The shift in S_a and S_q values are identical and with a difference of about 11% between Sa and S_q values. The linear relationship between the roughness and the strain existed until stress level of 0.45 was reached. At this point the roughness parameters experienced a slight reduction until the work piece finally failed. This deviation can be attributed to the deformation induced thinning of the thickness at the vicinity of the pole that is being considered; this will create an obstruction to grain rotation thereby leading to the stretching of the grain boundaries. However, the results for Sz and Sv in Fig. 9 shows that the roughness stayed uniform from this point until the material fails. This shows that the variation in peaks and valleys at these strains are negligible. Also, these changes can be explained on the basis of the Hall-Petch relationship [23]. Mismatching of grains, especially due to the sizing, tends to increase the roughness S_z. That is to say that the formation of smaller grains as a result of deformation will produces more mismatched points resulting in increases in roughness. However, as the thickness continues to decrease, the Hall-Petch relation begins to be ineffective in describing the stress-grain size relation. At this stage the reverse Hall-Petch starts to occur, and the grains begin to increase in size. This agrees with other works which submitted that a linear relationship exists between strain and roughness. According to [17], the smaller grains tend to encourage the roughening of surface. From Fig. 7 it can be deduced that as the pressure increases in hydraulic bulge tests, the thinning increased, especially near the pole of the bulge. In this region, the bulge is in state of plane stress and the rotation of grains occurs in this region as the stress increases.

The S_{sk} shows the degree of symmetry of the surface height about the mean plane. It indicates the distribution of peaks or valleys on a surface. This parameter describes the asperities of a surface hence, it has a direct impact on properties that are dependent on contact of surfaces such as interfacial contact resistivity. When is S_{sk} less than 0, it shows that the roughness is biased towards the peaks, while S_{sk} greater than 0 indicates a bias towards the valley. The S_{ku} value is a measure of the degree of sharpness of the roughness profile. If S_{ku} is less than 3, then the surface profile is free of extreme peaks and valleys and values of S_{ku} greater than 3 indicates the presence of numerus high peaks and valleys. Mathematically, the S_{sk} and S_{ku} are represented by Equations (3) and (4) respectively.

$$S_{sk} = \frac{1}{S_q^3} \iint_a Z(x,y)^3\,dx\,dy \quad (4)$$

$$S_{ku} = \frac{1}{S_q^4} \iint_a Z(x,y)^4\,dx\,dy \quad (5)$$

Fig. 10 shows the plot of Surface parameters S_{sk} and S_{ku}. The parameter S_{sk} stays uniform in the vicinity of negative as the strain increases and becomes slightly more negative as the work piece approaches failure. This is an indication that the number of peaks and valleys on the roughness profile remains constant as strain increases to about 0.45 and subsequently as strain increases towards failure more valleys were created. This observation supports the hypothesis that surface roughening is the result of rotation and mismatching of grains because peaks created by the mismatch of grains will be accompanied by valleys. The changes observed towards failure are associated with cold working induced microstructural evolution in the form stretching and breaking up of the grain boundaries to form smaller grains. The S_{ku} in the vicinity of 3 (S_{ku} = 3) suggests that there is symmetry on the roughness profile and the value is uniform until close to failure when an increase in is recorded which can be attributed to thinning at the pole of the workpiece.

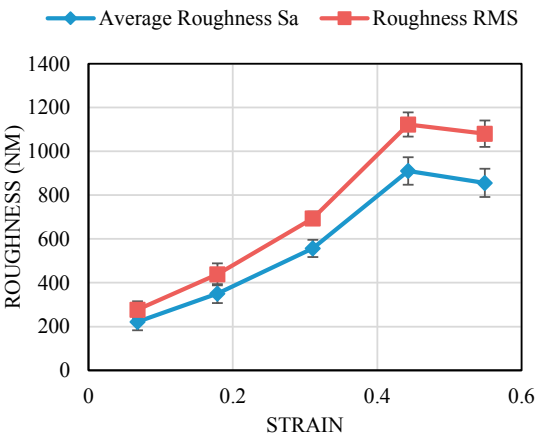

Fig. 8. The plot of roughness parameters (S_a and S_q) as a function of strain.

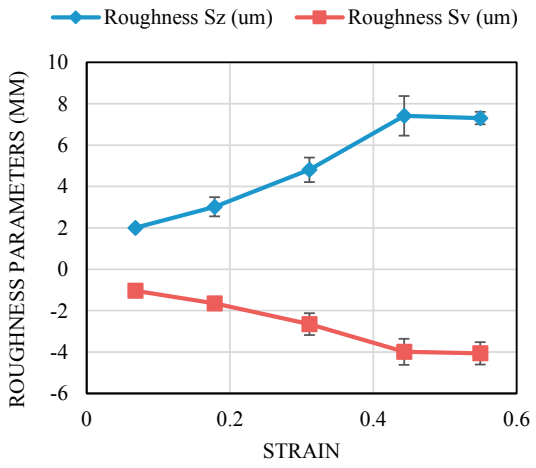

Fig. 9. The plot of roughness (S_v and S_z) as a function of the strain.

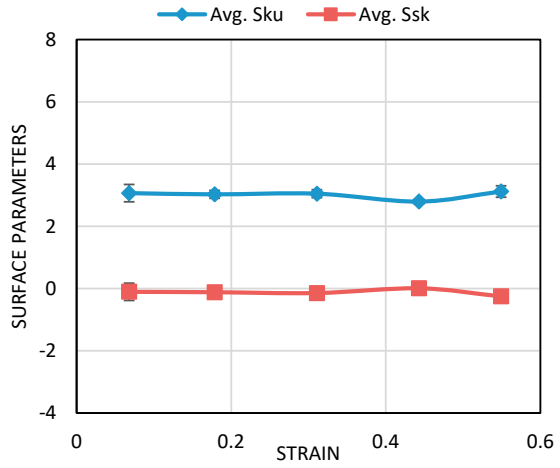

Fig. 10. Plot of skewness and kurtosis of the surface for various strains.

4.0 Summary and Conclusions

This work evaluated the variations of the surface roughness of AISI 304 stainless steel with respect to small macroscale to microscale regions of the hydroformed bulges in order to characterize the potential functional behavior of metallic bipolar plates prior to manufacturing. Hence, a thorough description of the surface quality of bulged hydroformed sheet metal with respect to local strain provides an avenue for integrating a predictive tool for surface roughness through such techniques add-on processes for FEA models while designing and manufacturing low cost metallic bipolar plates for proton exchange membrane fuel cells. The results of this work can be summarized as follows:

(i) The roughness (S_a and S_q.) increased with the increase in strain while bulging the workpieces. In addition, the largest peak height value (S_z) for the area under consideration increased with increasing strain while the absolute value of deepest pit (S_v) within the defined area appears also have increased.

(ii) This work shows that deformation and induced roughness follows a linear relationship both in microscale and macroscale. Considering that the area evaluated for this work was 2 mm by 2 mm square, the results show a similar relationship as the result shown by Olayinka et al. [9] where microscale scale areas were evaluated.

(iii) As a result of the work piece in the high strain regions, such as the pole of the bulge which are not in contact with the tooling, the Skewness (S_{sk}) and the Kurtosis (S_{ku}) of the 3-D surface texture that defines the degree of symmetry and presence of overly high peaks and valleys when characterizing the roughness in the workpieces are relatively constant with respect to strain resulting from hydroforming processes.

From these observations, it can be concluded that some of the roughness characteristics of bipolar plates that are a function of increased strain will be beneficial to the manufacturing and performance of low cost bipolar plates. These relationships were demonstrated for AISI 304 stainless steel sheet and may be incorporated into manufacturing simulations. Furthermore, testing for other materials may be useful when considering alternatives to AISI 304.

Hence, the cost of part rejection due to poor surface finish may be reduced which will in turn reduce the cost of producing metallic bipolar plates for proton exchange fuel cells. Evaluating surface roughness characteristics prior to manufacturing tooling will improve the process and tooling optimization for sheet hydroforming bipolar plates. Finally, it is important to note that while it is desirable to have many evenly distributed peaks in the roughness of the formed sheet metal which could be beneficial in achieving favorable electrical and thermal contact resistance, the resulting increased valleys due to increased roughness is detrimental to the robustness of metallic bipolar plates in fuel cells. Valleys may result localized corrosion such as pitting and crevice corrosion as well as disrupt the easy of flow of water, hydrogen, and oxygen, thereby resulting in the PEMFC over heating as a result of poor water management in the bipolar plates.

Therefore, it is important to create a favorable balance between the peaks and valleys that characterize the roughness of the workpieces resulting from the manufacture of bipolar plates. Lastly, the result of the skewness and kurtosis justified the use of sheet hydroforming technique for the manufacture of low-cost bipolar plate.

References

[1] Masuzawa, T. (2000). State of the art of micromachining. CIRP Annals—Manufacturing Technology 49(2):473–488

[2] Geiger, M., Vollertsen, F., and Kals, R. (1996). Fundamentals on the manufacturing of sheet metal microparts. *Annals of the CIRP,* 45(1), 227-282.

[3] Geiger, M., Kleiner, M., Eckstein, R., Tiesler, N. and Engel, U. (2001). Microforming, *CIRP A*nnals - Manufacturing Technology*,* 50, 445-462.

[4] Forouhandeh, F., Kumar, S., Ojha, S. N., & Balasubramanian, R. (2013). Recent developments in micro hydroforming. *Advances in Mechanical Engineering,* doi.org/10.1155/207165

[5] Luo, L., Jiang, Z., Wei, D., and He, X. (2014). Study on micro hydroforming of metals, Advanced Materials Research, Vols. 887-888, pp. 1133-1138.

[6] Hartl, C., Herwig Schiefer, H., and Chlynin, A. (2014). Evaluation of experimental and numerical investigations into micro-hydroforming of platinum tubes for an industrial application, Manufacturing Rev., 1 (2014) 17 DOI: https://doi.org/10.1051/mfreview/2014015

[7] Emblom, W.J., Wagner, S., Aithal, M., Ibne Islam, Md. F.S., Jones, R.J., and Glass, G.A., (2014). The development of a microscale strain measurement system applied to sheet bulge hydroforming, Journal of Manufacturing Process, http://dx.doi.org/10.1016/j.jmapro.2014.02.001.

[8] Kals, T.A., Eckstein R. (2000). Miniaturization in sheet metal working, Journal of Materials Processing Technology, v. 103, pp. 95-101.

[9] Olayinka, A., Emblom, W.J., Pasacreta, T.C., and Wagner, S.W. (2017). The effect of hydraulic bulge process on the surface topography of annealed AISI 304 stainless steel. Procedia Manufacturing 10 2017, 243 – 252

[10] Timoshevskii, V., Ke, Y., Guo*, H., and* Gall, D. (2008). The influence of surface roughness on electrical conductance of thin Cu films: An *ab initio* study, Journal of Applied Physics, Volume 103, Issue 11

[11] Meng, B., Fu, M.W. (2015). Size effect on deformation behavior and ductile fracture in micro forming of pure copper sheets considering free surface roughening

[12] Meng, B., Wan, M., and Cheng, C. (2017). Size effect on the forming limit of sheet metal in micro-scaled plastic deformation considering free surface roughening, Procedia Engineering 207:1010-1015.

[13] Raabe, D., Sachtleber, M., Weiland H., Scheele G., and Zhao Z. (2003) Grain-scale micromechanics of polycrystal surfaces during plastic straining, Acta Mater. 51 1539–1560.

[14] Raabe, D., Zhao Z., Sachtleber, M. (2002) Experimental investigation of plastic grain interaction, Materials Science and Engineering A336 81–87

[15] Rossiter, J., Brahme, A., Mishra, R. (2010). A new crystal plasticity scheme for explicit time integration codes to simulate deformation in 3D microstructures: Effects of strain path, strain rate and thermal softening on localized deformation in the aluminum alloy 5754 during simple shear, International Journal of Plasticity 26(12):1702-1725

[16] Stoudt, M.R., Levine, L.E., Creuziger, A., and Hubbard J.B. (2011). The fundamental relationships between grain orientation, deformation-induced surface roughness and Strain localization in an aluminum alloy," Materials Science and Engineering 530 (2011) 107–116

[17] Taylor, G.I. (1938). Plastic Strain in Metals," Journals of Institute of Metals. 62 307–324.

[18] Dieter G.E. (1986) Mechanical Metallurgy, McGraw-Hill, NewYork, USA

[19] Hertzberg, R.W., Vinci, R.P., and Hertzberg, J.L. (2012). Deformation and Fracture Mechanics of Engineering Materials, Wiley; 5th edition, ISBN: 978-0-470-52780-1

[20] Ashby, M.F., and Frost, H.J. (1982). Deformation-mechanism maps: the plasticity and creep of metals and ceramics, Pergamon Press, Oxford, p. 166.

[21] Alo, O. A., Otunniyi, I. O., and Pienaar, H. (2019). Manufacturing methods for metallic bipolar plates for polymer electrolyte membrane fuel cell, Materials and Manufacturing Processes, 34:8, 927-955

[22] Olayinka, A., Emblom, W.J., and Wagner, Scott W.(2017). Analytical and experimental evaluation of flow characteristics of annealed AISI 304 stainless steel sheet in multi-scale bulge forming." *Proceedings of the ASME 2017 12th International Manufacturing Science and Engineering Conference collocated with the JSME/ASME 2017 6th International Conference on Materials and Processing. Volume 1: Processes*.https://doi.org/10.1115/MSEC2017-2826.

[23] Petch N.J. (1953). The Cleavage strength of polycrystals, Journal. Iron Steel Institute. 174 (1953) 25–28